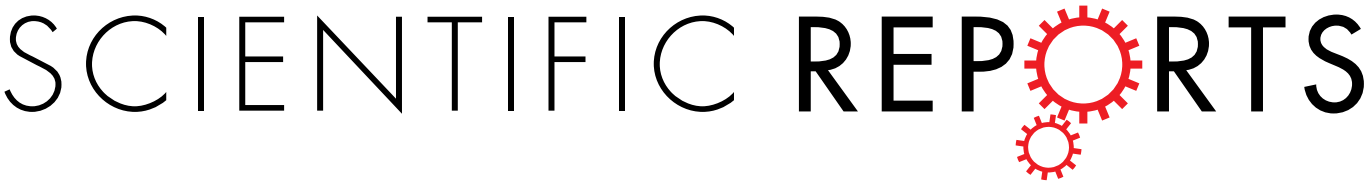

OPEN

Surface-Enhanced Raman Spectroscopy Assisted by Radical Capturer for Tracking of Plasmon-Driven Redox Reaction

Received: 06 April 2016
Accepted: 30 June 2016
Published: 22 July 2016

Xuefeng Yan, Lingzhi Wang, Xianjun Tan, Baozhu Tian & Jinlong Zhang

The deep understanding about the photocatalytic reaction induced by the surface plasmon resonance (SPR) effect is desirable but remains a considerable challenge due to the ultrafast relaxation of hole-electron exciton from SPR process and a lack of an efficient monitoring system. Here, using the p-aminothiophenol (PATP) oxidation SPR-catalyzed by Ag nanoparticle as a model reaction, a radical-capturer-assisted surface-enhanced Raman spectroscopy (SERS) has been used as an *in-situ* tracking technique to explore the primary active species determining the reaction path. Hole is revealed to be directly responsible for the oxidation of PATP to p, p′-dimercaptoazobenzene (4, 4′-DMAB) and O_2 functions as an electron capturer to form isolated hole. The oxidation degree of PATP can be further enhanced through a joint utilization of electron capturers of $AgNO_3$ and atmospheric O_2, producing p-nitrothiophenol (PNTP) within 10 s due to the improved hole-electron separation efficiency.

Decay of surface plasmon to hot carriers has found wide applications in energy conversion, photocatalysis and photodetection[1,2]. Among them, surface plasmonic resonance (SPR)-catalysed reactions have attracted increasing attention due to their green and convenient process[3,4]. Moreover, compared with the thermocatalysis, the SPR-catalysis often results in a unique selectivity[5–7]. However, due to the rapid relaxation process of hot carriers (hole and electron) on a short timescale ranging from femtosecond to picosecond, it is still hard to flexibly control the path/degree of SPR-catalysed reactions[8–10].

Deep and accurate understanding about the mechanism of SPR-catalysed reaction is highly essential for designing an efficient reaction system, which requires a sensitive and *in-situ* analysis strategy. Thanks for the same origin of SPR-catalysed reaction and surface-enhanced Raman spectroscopy (SERS) with an ultrahigh sensitivity up to single-molecule level, SERS is allowed to *in-situ* monitor the SPR-catalysed reaction process through providing fingerprint spectra of surface species[11–16]. Some theoretical and indirect experiment proofs from SERS have assumed the oscillated hot electrons and molecular O_2 are responsible for the SPR-catalysed redox reactions[17,18]. However, the active species determining the primary reaction step have still not been determined due to a lack of direct experimental proof.

Here, *in-situ* SERS technique aided with radical capturers for hot hole, electron and secondary radicals (•OH and $\bullet O_2^-$), generated from the plasmon decay of Ag nanoparticles (NPs), has unprecedentedly been used to determine the active species by adopting the oxidation of p-aminothiophenol (PATP) as a model reaction[19–22]. Hole is revealed to be directly responsible for the oxidation of PATP to p, p′-dimercaptoazobenzene (4, 4′-DMAB)[23,24]. Chu prepared Ag/TiO_2 system to investigate this reaction. The result shows that hot electrons generating from plasmonic decay would transfer to the conduction band of TiO_2, which enables the holes to trigger the immediate conversion[25]. The role of O_2 is determined as an electron capturer to produce isolated holes. PATP can be further oxidized to p-nitrothiophenol (PNTP) within 10 s through a joint utilization of electron capturers of $AgNO_3$ and atmospheric O_2[26,27]. To the best of our knowledge, this is the first time to unambiguously reveal the active species for the SPR-catalysed redox reaction through the *in-situ* SERS technique.

Key Laboratory for Advanced Materials and Institute of Fine Chemicals, East China University of Science and Technology, 130 Meilong Road, Shanghai 200237, P. R. China. Correspondence and requests for materials should be addressed to L.W. (email: wlz@ecust.edu.cn) or J.Z. (email: jlzhang@ecust.edu.cn)

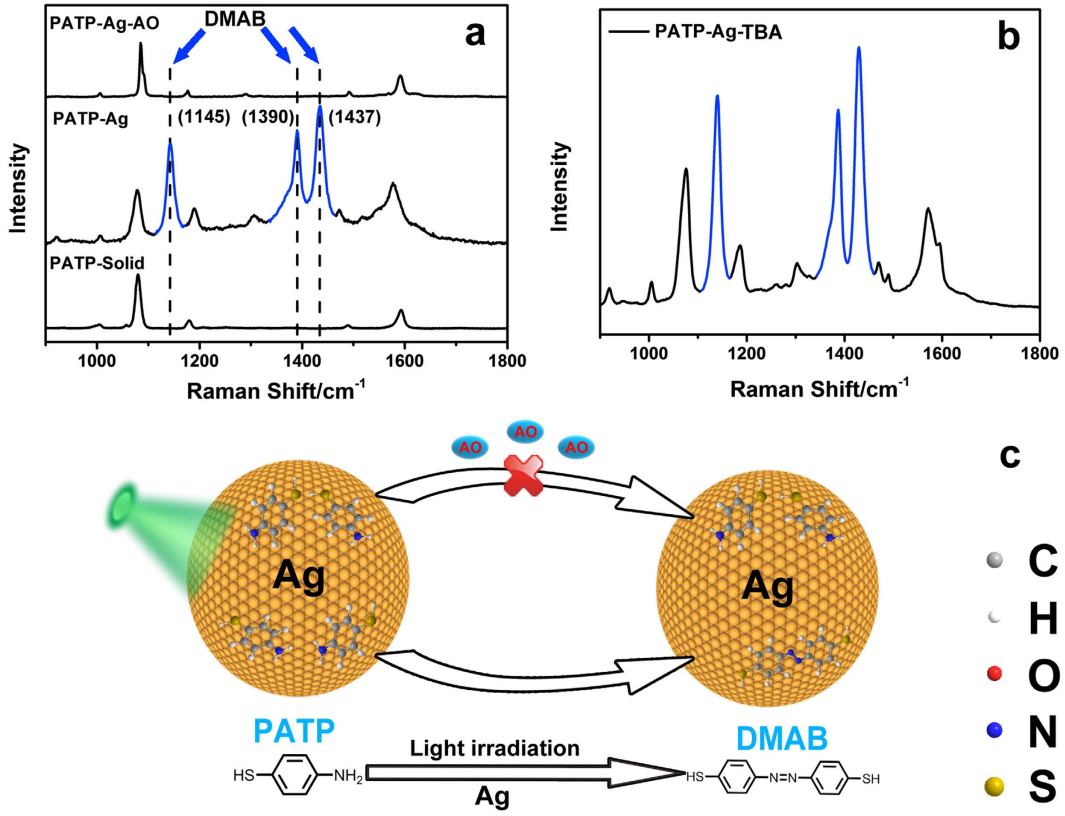

Figure 1. (**a**) Raman signal of PATP solid (black line), SERS signals of PATP on Ag nanoparticle layer in the absence and presence of AO; (**b**) SERS signal of PATP on assembly Ag nanoparticle layer in the presence of TBA; (**c**) Schematic diagram of plasmonic reactions on Ag layer in the presence of AO or TBA. Laser wavelength, 532 nm; Power, 2.5 mW; Integration time, 10 s.

Result and Discussion

Assembled Ag nanoparticle layer spin-coated from 50 nm of Ag NPs on a glass slide is used as plasmon-active substrate both for SERS analysis and catalysis reaction, which shows a wide plasmon resonance absorption band centred at 450 nm (Figures S1–S4). For assembled Ag nanoparticle layer adsorbed with PATP (Ag-PATP), Ag NPs and PATP are premixed before spin-coating. As shown in Fig. 1a, the SERS signal is collected under the irradiation of a 532 nm laser within 10 s. Compared with the Raman signal of PATP on the glass slide, three new peaks (blue line) assigned to the bend vibration of CH (β(CH)) at 1145 cm^{-1} and the stretching vibration of N = N (ν(N = N)) at 1390 and 1437 cm^{-1} are observed, implying PATP is oxidized to 4, 4′-DMAB as driven by the SPR effect of Ag nanoparticle layer[28–34]. All the three strongly enhanced peaks of DMAB represent symmetric a_g vibrational modes, strongly indicating the formation of DMAB from PATP through the N = N bond. These peaks are assigned to the a_{g12}, a_{g16}, and a_{g17} symmetric vibrational modes, respectively[35,36]. However, it is found that when ammonium oxalate (AO), a commonly used hole capturer is present, the reaction from PATP to 4, 4′-DMAB is completely quenched since no signal from 4, 4′-DMAB is observed. This result indicates the capturer-assisted strategy actually allows SERS to *in-situ* explore the reaction process in spite of the ultrafast relaxation process of hot carriers. Since both hole and its secondary radical •OH are strong oxidants, it still cannot be distinguished that PATP is oxidized by hole or •OH. Therefore, t-butanol (TBA) as the capturer for •OH is further adopted to understand its influence on the reaction[37]. However, strong peaks attributed to 4, 4′-DMAB is still observed with preserved intensity, suggesting the reaction from PATP to 4, 4′-DMAB is not altered by •OH (Fig. 1b). Therefore, it is undoubted that the oxidation of PATP is directly related to the hole decayed from the surface plasmon resonance of Ag nanoparticle layer. To get the original spectrum of PATP, it also can be detected on the Ag substrate by the irradiation of 785 nm on lower laser powers such as 0.50 μW and 0.25 mW (Figure S5).

The above results seem to be inconsistent with the current reports, where the hot electron together with oxygen is generally considered to be responsible for the plasmon-driven oxidation reaction[38,39]. To reveal the real role of oxygen and electron during the oxidation of PATP, the reaction was further carried out in N_2 atmosphere (Fig. 2a), which is significantly prohibited, suggesting O_2 indeed contributes to the oxidation of PATP. It is highly possible that O_2 may be reduced by hot electron to $\bullet O_2^-$ with strong oxidation capacity, which further cause the oxidation of PATP. To check this conjecture, a typical $\bullet O_2^-$ capturer, p-benzoquinone (BQ), is further applied in the SERS analysis. However, the synthesis conducted in the atmospheric environment in the presence of BQ does not cause any variation of 4, 4′-DMAB signals (Fig. 2b), excluding the possible effect of $\bullet O_2^-$ on the oxidation of PATP. Intriguingly, when $AgNO_3$ is adopted as an electron capturer in N_2 atmosphere, the oxidation of PATP to 4, 4′-DMAB occurs even in the absence of oxygen. A similar experiment was conducted in the water solution[40–43]

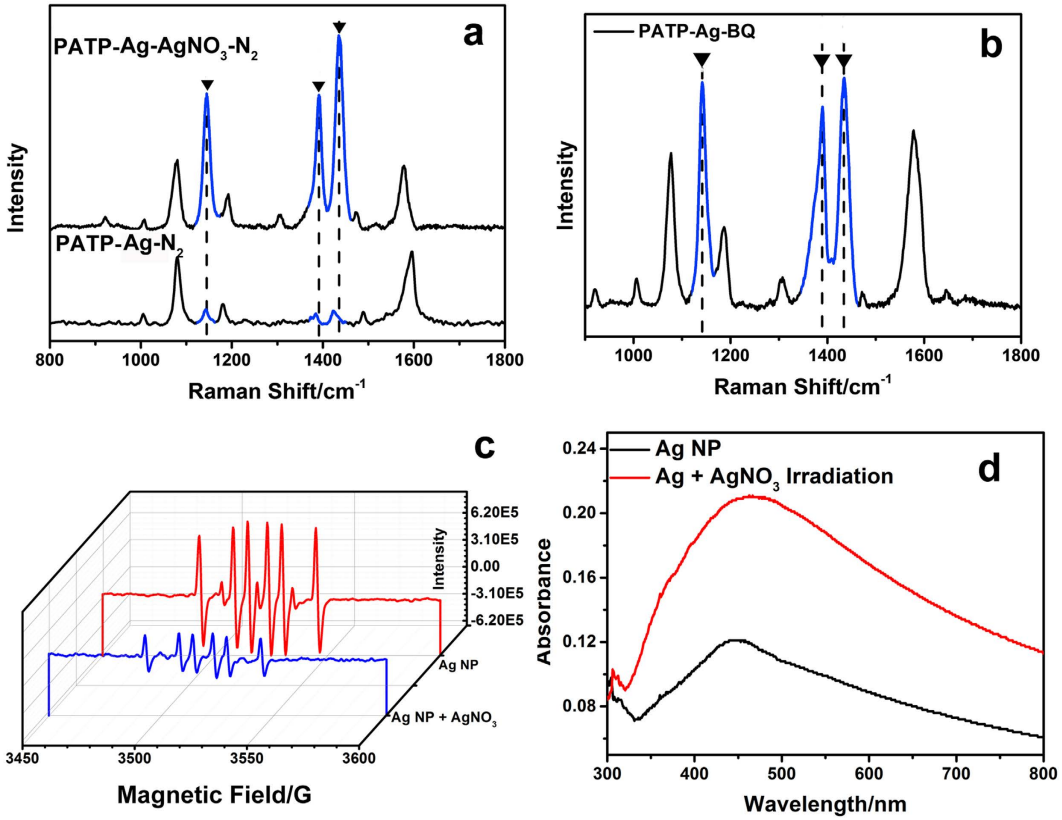

Figure 2. (**a**) SERS signals of PATP on Ag and Ag-$AgNO_3$ substrates in N_2 atmosphere; (**b**) SERS signals of PATP in the presence of BQ; (**c**) EPR spectra of DMPO on Ag nanoparticles in the absence and presence of $AgNO_3$; (**d**) UV-Vis spectra of Ag-$AgNO_3$ substrates before and after the light irradiation. The characteristic peaks of 4, 4′-DMAB labelled by ▼.

and the result confirm our suppose (Figure S6). As figure shows, in the water solution, the hole sacrificial agent AO is useful to prohibit the generation of DMAB. And the signal intensity of detected molecule seems weaker for the poor plasmon in the solution.

Electron spin resonance (ESR) is then further adopted to analyse the function of $AgNO_3$ in the oxidation of PATP by using 5, 5-dimethyl-1-pyrroline N-oxide (DMPO) as the indicator of $\bullet O_2^-$. It is obvious that the intense signal appears on Ag nanoparticle layer under the laser irradiation, but the presence of $AgNO_3$ causes the decreased peak intensity of DMPO-$\bullet O_2^-$ (Fig. 2c), which thus proves two facts as follows. First, O_2 adsorbed on the surface of Ag nanoparticle layer can actually be reduced by SPR-derived electron. However, the presence of superoxide radical has no effect on the oxidation of PATP; Second, hot electrons can be indeed captured by $AgNO_3$ according to the retarded formation of $\bullet O_2^-$. Based on these two facts, the oxidation of PATP in the absence of O_2 should be attributed to the improved concentration of holes due to the capture of electron by $AgNO_3$ (eqs 1–3, SI).

Generally, the SPR-derived hole-electron exciton from Ag nanoparticle layer resides in the Fermi energy level, which is harder to be separated than that formed from semiconductor[44–49]. Since the hole has been revealed as the exclusively active species for the oxidation of PATP instead of O-containing oxidants, the retarded oxidation from PATP to 4, 4′-DMAB in the absence of O_2 should be attributed to the inefficient separation of hole from electron. As such, molecular O_2 should actually function as an electron capturer, which consumes electrons and produce enough holes to initiate the oxidation of PATP (eq 4, SI). Moreover, it is noted the plasmonic absorption of Ag nanoparticle layer in the presence of $AgNO_3$ (Ag-$AgNO_3$) is enhanced under UV-light irradiation (500 W Xe light, Fig. 2d), implying a possible reduction of $AgNO_3$ to Ag during the SERS analysis. To understand the influence of enhanced plasmon resonance intensity on the reaction, the SERS of PATP on the pre-irradiated Ag-$AgNO_3$ assembled nanoparticle layer has been further investigated in N_2 atmosphere. The signal intensity attributed to 4, 4′-DMAB seems too low to be detected (Figure S7), thus excluding the contribution from improved plasmon resonance intensity to the conversion efficiency.

Furthermore, it is found that when both of $AgNO_3$ and atmospheric O_2 are present, PATP is unprecedentedly transformed into a mixture of PNTP and 4, 4′-DMAB within 10 s as characterized by the appearance of ν (NO_2) peak at ca. 1330 cm^{-1} (Fig. 3a), demonstrating the oxidation efficiency can be enhanced by improving the separation degree of hole-electron exciton. Both of $AgNO_3$ and O_2 should be involved in the oxidation of 4, 4′-DMAB to PNTP since no PNTP can be produced when either of them is absent. The influence of $AgNO_3$ density (ρ_{Ag}) on the conversion efficiency was further investigated. It is found from Fig. 3a that 4, 4′-DMAB is the dominant product at a laser power of 0.5 mW and ρ_{Ag} of $2.3^{*}10^{-6}$ g/cm^2, as evidenced by the strong peaks at 1440, 1380 and

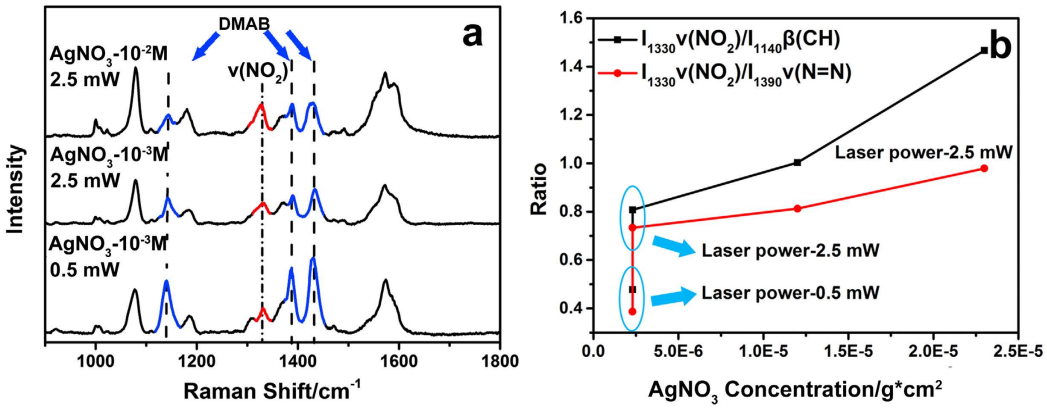

Figure 3. (**a**) SERS signals of PATP on Ag-$AgNO_3$ substrates under the irradiation of 532 nm laser light; (**b**) Relation between the density of $AgNO_3$ and the composition ratio of PNTP/4, 4′-DMAB.

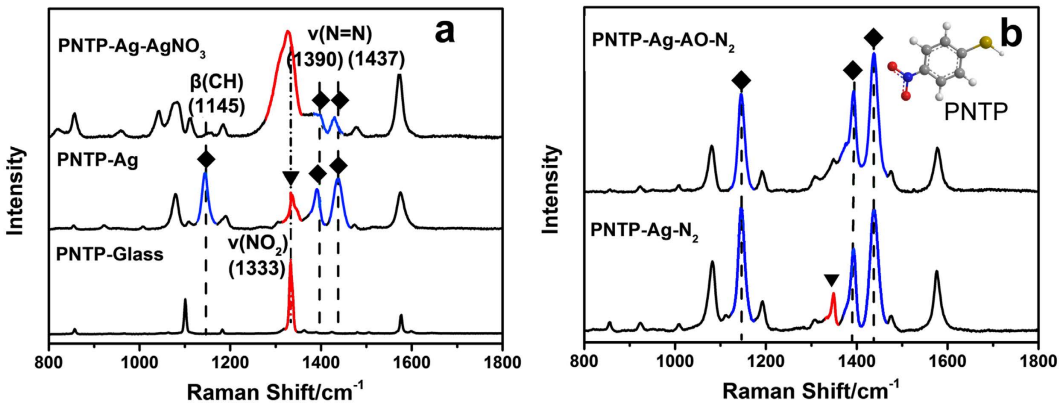

Figure 4. (**a**) Raman spectra of PNTP on the glass slide, SERS signals of PNTP on assemble Ag layer in the absence and presence of $AgNO_3$. (**b**) SERS signals of PNTP on the Ag and Ag-AO substrates in N_2 atmosphere.

1140 cm^{-1} from 4, 4′-DMAB and a weak peak at 1330 cm^{-1} due to the $\nu(NO_2)$ of PNTP. The peaks of 4, 4′-DMAB decreases when the laser power and ρ_{Ag} increase to 2.5 mW and $2.3*10^{-5}$ g/cm^2, along with an increasing intensity of ν (NO_2) peak. The intensity ratio between peaks at 1330 and 1390 cm^{-1} ($I_{1330}\nu(NO_2)/I_{1390}\nu(N=N)$) was plotted to more clearly demonstrate the co-effect of $AgNO_3$ and laser power (Fig. 3a, red line). The ratio of $I_{1330}\nu(NO_2)/I_{1140}\beta(CH)$ was also plotted and used as a reference (Fig. 3b, black line). The $I_{1330}\nu(NO_2)/I_{1390}\nu(N=N)$ and $I_{1330}\nu(NO_2)/I_{1140}\beta(CH)$ obtained at 2.5 mW are almost doubled compared with those formed at 0.5 mW when ρ_{Ag} is $2.3*10^{-6}$ g/cm^2, which are further improved for ca. 30% and 80% when ρ_{Ag} is increased to $2.3*10^{-5}$ g/cm^2. A higher ρ_{Ag} leads to the decreased intensity of both 4, 4′-DMAB and PNTP (not shown), implying the shielding of Ag nanoparticle layer by overmuch addition of $AgNO_3$. The actual composition of PNTP should be higher as valued from the peak intensity ratio between the a_1 and a_g modes since the intensities of the a_g modes of 4, 4′-DMAB are significantly stronger than those of the a_1 modes of PNTP[50], where a small amount of 4, 4′-DMAB may already produce observable signal in SERS spectra. What's more, to investigate the role of laser power and exposure time[51], Ag-$AgNO_3$ substrate was taken to detect PATP under 0.5 and 0.25 mW with different exposure times as Figure S8. The laser is both used for the light source of the SPR reaction and SERS analysis. The decreasing of the laser power decreases the reaction efficiency and so does the SERS sensitivity. We further investigated the reaction under 0.25 mW irradiation, where the Raman intensity is decreased without obvious variation of the reaction efficiency. The variation of the irradiation time to 5 s or 3 min does not obviously cause the change of the reaction process. However, when the exposure time extends to 10 min, the sample seems to be destroyed by the strong laser power, weakening the signal of the PNTP and DMAB on the substrate.

As a further check for the feasibility of radical-capture strategy to the *in-situ* SERS analysis of other SPR catalytic reactions, the SPR-catalysed reduction of PNTP, another typical reaction model has been further adopted here[31]. The results shown in Fig. 4a indicate the reduction of PNTP is retarded when $AgNO_3$ is present, accordant with the commonly-accepted understanding about the function of electrons in the SPR-catalysed reduction reaction[3,4]. On the contrary, the reduction can be promoted by conducting the reaction in N_2 atmosphere (Fig. 4b), which should be attributed to the eliminated consumption of electron by molecular O_2. Even more, a higher

reduction degree of PNTP is achieved when AO is adopted to improve the electron concentration through consuming more holes (Fig. 4b).

Conclusions

In summary, we have explored the mechanism of SPR-catalysed reaction by a capturer-assisted SERS strategy using the oxidation of PATP on Ag nanoparticle layer as the model reaction. The adoption of AO and $AgNO_3$ as the capturers for hole and electron effectively leads to the separation of SPR-derived hot holes and electrons. The hot hole is directly responsible for the oxidation of PATP to 4, 4′-DMAB. The oxidation of PATP is prohibited in N_2 atmosphere but occurs when $AgNO_3$ is further present. O_2 plays the role as an electron capturer in promoting the separation of hole-electron. The oxidation of PATP to PNTP has been unprecedentedly achieved in the atmospheric environment when the reaction is assisted by $AgNO_3$. This study provides a novel way to deeply understand the mechanism of plasmon-related photocatalysis and photochemical reactions, which is expected to substantially push the development of SPR-induced green synthesis forward through rational and scientific design.

Method

Experimental Section. *Preparation of Ag Nanoparticles with Diameter of ca. 50 nm.* The preparation of Ag nanoparticles is adopted from a previously reported method[52]. In a typical synthesis, 85.0 mg of PVP was dispersed into 20.0 mL of water under magnetic stirring. After the complete dissolution of PVP, 85.0 mg of $AgNO_3$ and 200 μL of 5.0 M NaCl were successively added under rapid stirring. The mixture was kept stirring in the dark for 15 min to form AgCl colloid. The freshly prepared AgCl colloid was then used as the precursor for Ag nanoparticles to achieve a size-controlled synthesis. First, 20.0 mL of 50.0 mM ascorbic acid was added to 2.5 mL of 0.5 M NaOH under magnetic stirring, and 2.5 mL of freshly prepared AgCl colloid is also added. The mixture was then stirred for 2 h in the dark. The products are collected by centrifugation and washed with water and kept in an ethanol solution.

Preparation of assembled Ag nanoparticle layer. Assembled Ag nanoparticle layer was spin-coated from the ethanol solution of Ag nanoparticles (1.0 mL, 0.05 M) and used for SEM, AFM and UV-Vis diffuse reflectance analyses. PNTP or PATP (200 μL, 10^{-2} M) was dispersed on Ag nanoparticle layer by premixing the molecules with the Ag ethanol solution and the mixture was spin-coated using the above procedure. For the study in the presence of capturing agent, 200 μL ethanol solution of $AgNO_3$, AO, CH_3OH and BQ (10^{-3}–10^{-2} M) was mixed with 200 μL PNTP or PATP solution (10^{-2} M) before the spin-coating process.

Characterization. Scanning electron microscopy (SEM) analysis was performed using a TESCAN nova III scanning electron microscope. Transmission electron microscopy (TEM) analysis was performed using a JEOL 2100 LaB6 TEM, at a 200 kV accelerating voltage. Raman spectra were recorded on a Renishaw inVia-Reflex Raman microprobe system equipped with Peltier charge-coupled device (CCD) detectors and a Leica microscope. Spectra were collected from the nanoparticle layer with an accumulation time of 10 s. Lasers with wavelength of 532 nm and 785 nm were used as the excitation light source, and a 50× objective with a numerical aperture (NA) of 0.75 was used to get the laser spot diameter of ~1 μm. The electron spin resonance (ESR) technique (with DMPO) was used to detect the radical species over the catalyst on a Bruker EMX-8/2.7 spectrometer. DMPO was added to the suspension system before testing, and then the system was irradiated by visible light using a Xenon lamp. Electron spin resonance (ESR) technique is a very powerful and sensitive method for the characterization of the electronic structures of materials with unpaired electrons. By investigating the resonance line can obtain the information about status of the unpaired electrons in radical and its surrounding environmental, thereby obtaining information about the structure and chemical bonding of the substance, in order to identify the different types of free radicals and their levels.

References

1. Fuku, K. *et al.* The synthesis of size- and color-controlled silver nanoparticles by using microwave heating and their enhanced catalytic activity by localized surface plasmon resonance. *Angewandte Chemie* **52,** 7446–7450 (2013).
2. Brongersma, M. L., Halas, N. J. & Nordlander, P. Plasmon-induced hot carrier science and technology. *Nat Nanotechnol* **10,** 25–34 (2015).
3. Wang, J., Ando, R. A. & Camargo, P. H. Controlling the selectivity of the surface plasmon resonance mediated oxidation of p-aminothiophenol on Au nanoparticles by charge transfer from UV-excited TiO_2. *Angewandte Chemie* **54,** 6909–6912 (2015).
4. Zhao, L.-B. *et al.* Theoretical study of plasmon-enhanced surface catalytic coupling reactions of aromatic amines and nitro Compounds. *The Journal of Physical Chemistry Letters* **5,** 1259–1266 (2014).
5. Lang, X., Chen, X. & Zhao, J. Heterogeneous visible light photocatalysis for selective organic transformations. *Chemical Society reviews* **43,** 473–486 (2014).
6. Naya, S., Inoue, A. & Tada, H. Self-assembled heterosupramolecular visible light photocatalyst consisting of gold nanoparticle-loaded titanium(IV) dioxide and surfactant. *J Am Chem Soc* **132,** 6292–6293 (2010).
7. Kubacka, A., Fernandez-Garcia, M. & Colon, G. Advanced nanoarchitectures for solar photocatalytic applications. *Chem Rev* **112,** 1555–1614 (2012).
8. Mubeen, S. *et al.* An autonomous photosynthetic device in which all charge carriers derive from surface plasmons. *Nat Nanotechnol* **8,** 247–251 (2013).
9. Kubo, A., Pontius, N. & Petek, H. Femtosecond microscopy of surface plasmon polariton wave packet evolution at the silver/vacuum interface. *Nano letters* **7,** 470–475 (2007).
10. Kubo, A. *et al.* Femtosecond imaging of surface plasmon dynamics in a nanostructured silver film. *Nano letters* **5,** 1123–1127 (2005).
11. Qian, X., Li, J. & Nie, S. Stimuli-responsive SERS nanoparticles: conformational control of plasmonic coupling and surface Raman enhancement. *J Am Chem Soc* **131,** 7540–7541 (2009).
12. Qi, D., Lu, L., Wang, L. & Zhang, J. Improved SERS sensitivity on plasmon-free TiO_2 photonic mi-croarray by enhancing light-matter coupling. *Journal of the American Chemical Society* (2014).

13. Huang, J. *et al.* Site-specific growth of Au-Pd alloy horns on Au nanorods: a platform for highly sensitive monitoring of catalytic reactions by surface enhancement Raman spectroscopy. *J Am Chem Soc* **135,** 8552–8561 (2013).
14. Yan, X. *et al.* Sensitive and easily recyclable plasmonic SERS substrate based on Ag nanowires in mesoporous silica. *RSC Adv.* **4,** 57743–57748 (2014).
15. Chen, C., Ma, W. & Zhao, J. Semiconductor-mediated photodegradation of pollutants under visible-light irradiation. *Chemical Society reviews* **39,** 4206–4219 (2010).
16. Ingram, D. B., Christopher, P., Bauer, J. L. & Linic, S. Predictive model for the design of plasmonic metal/semiconductor composite photocatalysts. *ACS Catalysis* **1,** 1441–1447 (2011).
17. Zhao, L.-B., Chen, J.-L., Zhang, M., Wu, D.-Y. & Tian, Z.-Q. Theoretical study on electroreduction of p-nitrothiophenol on silver and gold electrode surfaces. *The Journal of Physical Chemistry C* **119,** 4949–4958 (2015).
18. Xu, P. *et al.* Mechanistic understanding of surface plasmon assisted catalysis on a single particle: cyclic redox of 4-aminothiophenol. *Scientific reports* **3,** 2997 (2013).
19. Lin, W.-C., Yang, W.-D., Huang, I. L., Wu, T.-S. & Chung, Z.-J. Hydrogen production from methanol/water photocatalytic decomposition using Pt/$TiO_{2-x}N_x$ Catalyst. *Energy & Fuels* **23,** 2192–2196 (2009).
20. Schneider, J. & Bahnemann, D. W. Undesired role of sacrificial reagents in photocatalysis. *The Journal of Physical Chemistry Letters* **4,** 3479–3483 (2013).
21. Tian, X., Chen, L., Xu, H. & Sun, M. Ascertaining genuine SERS spectra of p-aminothiophenol. *RSC Advances* **2,** 8289 (2012).
22. Zhang, Z., Xu, P., Yang, X., Liang, W. & Sun, M. Surface plasmon-driven photocatalysis in ambient, aqueous and high-vacuum monitored by SERS and TERS. *Journal of Photochemistry and Photobiology C: Photochemistry Reviews* 10.1016/j.jphotochemrev.2016.04.001 (2016).
23. Lee, M. C. & Choi, W. Solid phase photocatalytic reaction on the soot/TiO_2 interface: the role of migrating OH radicals. *The Journal of Physical Chemistry B* **106,** 11818–11822 (2002).
24. Xu, T., Zhang, L., Cheng, H. & Zhu, Y. Significantly enhanced photocatalytic performance of ZnO via graphene hybridization and the mechanism study. *Applied Catalysis B: Environmental* **101,** 382–387 (2011).
25. Chu, J. *et al.* Ultrafast surface-plasmon-induced photodimerization of p-aminothiophenol on Ag/TiO_2 nanoarrays. *ChemCatChem* **8,** 1–7 (2016).
26. van Schrojenstein Lantman, E. M., Deckert-Gaudig, T., Mank, A. J., Deckert, V. & Weckhuysen, B. M. Catalytic processes monitored at the nanoscale with tip-enhanced Raman spectroscopy. *Nat Nanotechnol* **7,** 583–586 (2012).
27. Wu, D.-Y. *et al.* Surface catalytic coupling reaction of p-mercaptoaniline linking to silver nanostructures responsible for abnormal SERS enhancement: A DFT Study. *The Journal of Physical Chemistry C* **113,** 18212–18222 (2009).
28. Qi, D., Yan, X., Wang, L. & Zhang, J. Plasmon-free SERS self-monitoring of catalysis reaction on Au nanoclusters/TiO_2 photonic microarray. *Chemical communications* **51,** 8813–8816 (2015).
29. Naya, S., Niwa, T., Kume, T. & Tada, H. Visible-light-induced electron transport from small to large nanoparticles in bimodal gold nanoparticle-loaded titanium(IV) oxide. *Angewandte Chemie* **53,** 7305–7309 (2014).
30. Zhu, H., Ke, X., Yang, X., Sarina, S. & Liu, H. Reduction of nitroaromatic compounds on supported gold nanoparticles by visible and ultraviolet light. *Angewandte Chemie* **49,** 9657–9661 (2010).
31. Dong, B., Fang, Y., Chen, X., Xu, H. & Sun, M. Substrate-, wavelength-, and time-dependent plasmon-assisted surface catalysis reaction of 4-nitrobenzenethiol dimerizing to p, p′-dimercaptoazobenzene on Au, Ag, and Cu films. *Langmuir: the ACS journal of surfaces and colloids* **27,** 10677–10682 (2011).
32. Fang, Y., Li, Y., Xu, H. & Sun, M. Ascertaining p, p′-dimercaptoazobenzene produced from p-aminothiophenol by selective catalytic coupling reaction on silver nanoparticles. *Langmuir: the ACS journal of surfaces and colloids* **26,** 7737–7746 (2010).
33. Huang, Y., Fang, Y., Yang, Z. & Sun, M. Can p, p′-dimercaptoazobisbenzene be produced from p-aminothiophenol by surface photochemistry reaction in the junctions of a Ag nanoparticle–molecule−Ag (or Au) film? *The Journal of Physical Chemistry C* **114,** 18263–18269 (2010).
34. Sun, M. & Xu, H. A novel application of plasmonics: plasmon-driven surface-catalyzed reactions. *Small* **8,** 2777–2786 (2012).
35. Zhang, Z., Fang, Y., Wang, W., Chen, L. & Sun, M. Propagating surface plasmon polaritons: towards applications for remote-excitation surface catalytic reactions. *Advanced Science* **3,** 1500215 (2016).
36. Sun, M., Fang, Y., Zhang, Z. & Xu, H. Activated vibrational modes and Fermi resonance in tip-enhanced Raman spectroscopy. *Physical review. E, Statistical, nonlinear, and soft matter physics* **87,** 020401 (2013).
37. Pan, X. & Xu, Y.-J. Defect-mediated growth of noble-metal (Ag, Pt, and Pd) nanoparticles on TiO_2 with oxygen vacancies for photocatalytic redox reactions under visible light. *The Journal of Physical Chemistry C* **117,** 17996–18005 (2013).
38. Huang, Y. F. *et al.* Activation of oxygen on gold and silver nanoparticles assisted by surface plasmon resonances. *Angewandte Chemie* **53,** 2353–2357 (2014).
39. Huang, Y. F. *et al.* When the signal is not from the original molecule to be detected: chemical transformation of para-aminothiophenol on Ag during the SERS measurement. *J Am Chem Soc* **132,** 9244–9246 (2010).
40. Ding, Q., Chen, M., Li, Y. & Sun, M. Effect of aqueous and ambient atmospheric environments on plasmon-driven selective reduction reactions. *Scientific reports* **5,** 10269 (2015).
41. Cui, L., Wang, P., Li, Y. & Sun, M. Selective plasmon-driven catalysis for para-nitroaniline in aqueous environments. *Scientific reports* **6,** 20458 (2016).
42. Cui, L., Wang, P., Fang, Y., Li, Y. & Sun, M. A plasmon-driven selective surface catalytic reaction revealed by surface-enhanced Raman scattering in an electrochemical environment. *Scientific reports* **5,** 11920 (2015).
43. Cui, L. *et al.* Plasmon-driven catalysis in aqueous solutions probed by SERS spectroscopy. *Journal of Raman Spectroscopy* doi: 10.1002/jrs.4939 (2016).
44. Linic, S., Christopher, P. & Ingram, D. B. Plasmonic-metal nanostructures for efficient conversion of solar to chemical energy. *Nature materials* **10,** 911–921 (2011).
45. Christopher, P., Xin, H. & Linic, S. Visible-light-enhanced catalytic oxidation reactions on plasmonic silver nanostructures. *Nature chemistry* **3,** 467–472 (2011).
46. Warren, S. C. & Thimsen, E. Plasmonic solar water splitting. *Energy Environ. Sci.* **5,** 5133–5146 (2012).
47. Enache, D. I. *et al.* Solvent-free oxidation of primary alcohols to aldehydes using Au-Pd/TiO_2 catalysts. *Science* **311,** 362–365 (2006).
48. Corma, A. & Serna, P. Chemoselective hydrogenation of nitro compounds with supported gold catalysts. *Science* **313,** 332–334 (2006).
49. Tsukamoto, D. *et al.* Gold nanoparticles located at the interface of anatase/rutile TiO_2 particles as active plasmonic photocatalysts for aerobic oxidation. *J Am Chem Soc* **134,** 6309–6315 (2012).
50. Futamata, M. Surface-plasmon-polariton-enhanced Raman scattering from self-assembled monolayers of p-nitrothiophenol and p-aminothiophenol on silver. *The Journal of Physical Chemistry* **99,** 11901–11908 (1995).
51. Sun, M., Zhang, Z., Zheng, H. & Xu, H. *In-situ* plasmon-driven chemical reactions revealed by high vacuum tip-enhanced Raman spectroscopy. *Scientific reports* **2,** 647 (2012).
52. Chen, B., Jiao, X. & Chen, D. Size-controlled and size-designed synthesis of nano/submicrometer Ag particles. *Crystal Growth & Design* **10,** 3378–3386 (2010).

Acknowledgements

This work has been supported by the National Natural Science Foundation of China (21173077, 21377038 and 21237003, 21203062), the National Basic Research Program of China (973 Program, 2013CB632403), the Research Fund for the Doctoral Program of Higher Education (20120074130001) and the Fundamental Research Funds for the Central Universities.

Author Contributions

X.Y. designed and performed the experiments, prepared the manuscript, drawing and subsequent edit/improvement. X.T. performed the Raman characteristics. L.W., B.T. and J.Z. proposed the research direction and guided the project. All authors discussed the results and commented on the manuscript.

Additional Information

Supplementary information accompanies this paper at http://www.nature.com/srep

Competing financial interests: The authors declare no competing financial interests.

How to cite this article: Yan, X. *et al.* Surface-Enhanced Raman Spectroscopy Assisted by Radical Capturer for Tracking of Plasmon-Driven Redox Reaction. *Sci. Rep.* **6**, 30193; doi: 10.1038/srep30193 (2016).